Published in final edited form as:
Biomech Model Mechanobiol. 2013 January ; 12(1): 5–17. doi:10.1007/s10237-012-0377-8.

Calcific nodule morphogenesis by heart valve interstitial cells is strain dependent

Charles I. Fisher[1,*], **Joseph Chen**[1,*], and **W. David Merryman**[1,#]
[1] Department of Biomedical Engineering Vanderbilt University, Nashville, TN

Abstract

Calcific aortic valve disease (CAVD) results in impaired function through the inability of valves to fully open and close, but the causes of this pathology are unknown. Stiffening of the aorta is associated with CAVD and results in exposing the aortic valves to greater mechanical strain. Transforming growth factor β1 (TGF-β1) is enriched in diseased valves and has been shown to combine with strain to synergistically alter aortic valve interstitial cell (AVIC) phenotypes. Therefore, we investigated the role of strain and TGF-β1 on the calcification of AVICs. Following TGF-β1 pretreatment, strain induced intact monolayers to aggregate and calcify. Using a wound assay, we confirmed that TGF-β1 increases tension in the monolayer in parallel with α-smooth muscle actin (αSMA) expression. Continual exposure to strain accelerates aggregates to calcify into mature nodules that contain a necrotic core surrounded by an apoptotic ring. This phenotype appears to be mediated by strain inhibition of AVIC migration after the initial formation of aggregates. To better interpret the extent to which externally applied strain physically impacts this process, we modified the classical Lamé solution, derived using principles from linear elasticity, to reveal strain magnification as a novel feature occurring in a mechanical environment that supports nodule formation. These results indicate that strain can impact multiple points of nodule formation: by modifying tension in the monolayer, remodeling cell contacts, migration, apoptosis, and mineralization. Therefore, strain induced nodule formation provides new directions for developing strategies to address CAVD.

Keywords

Calcific Aortic Valve Disease; Mechanobiology; TGF-β1; αSMA; Mechanical Strain; Apoptosis; Dystrophic Calcification; Aortic Valve Interstitial Cell; Myofibroblast

1. Introduction

Calcific aortic valve disease (CAVD) is the third leading cause of cardiovascular disease and is now the most common form of acquired valvular disease in industrialized countries (Roger et al. 2011; Goldbarg et al. 2007). Calcific aortic valves display impaired function through the inability to fully open and close, resulting in abnormal blood flow and increased load imparted to the myocardium (Merryman 2009). There are no current means of pharmacological intervention for CAVD, and the only effective treatment is surgical replacement (Helske et al. 2007; Goldbarg et al. 2007; Rajamannan 2010).

[#] For Correspondence: W. David Merryman, Ph.D. Biomedical Engineering Vanderbilt University david.merryman@vanderbilt.edu Office: 615-322-7219 Lab: 615-343-0009 Fax: 615-322-6541 Room 9445D MRB IV 2213 Garland Avenue Nashville TN 37232-0493.
[*] Co-first authors 9445 MRB IV 2213 Garland Ave. Nashville, TN 37232

The evolution of CAVD is hypothesized to be initiated by abnormal responses of aortic valve interstitial cells (AVICs), the residential cell type responsible for maintaining valve integrity (Merryman 2008). For example, AVIC aggregation and formation into calcific nodules have been useful *in vitro* model systems that have revealed various stimuli that cause these pathologic responses (Kennedy et al. 2009; Balachandran et al. 2010; Jian et al. 2003; Mohler et al. 1999; Yip et al. 2009; Benton et al. 2009). Because AVICs are greatly influenced by cytokines such as transforming growth factor-β1 (TGF-β1) and mechanical cues such as substrate composition and stiffness, these stimuli have been primarily studied and are thought to contribute to the pathology of CAVD. Specifically, TGF-β1 is a potent inducer of myofibroblast differentiation in AVICs and has been shown to be enriched in sclerotic valves and promotes calcification of *in vitro* cultures (Walker et al. 2004; Chen et al.). Substrate composition and interaction with AVIC integrins also regulates the likelihood of aggregation and calcification (Gu and Masters 2010; Benton et al. 2008; Cushing et al. 2005). AVIC differentiation can also be regulated mechanically *in vitro*; compliant substrates lead to AVIC differentiation into osteoblast-like cells which actively secrete bone matrix, while stiff substrates lead to myofibroblast differentiation (Yip et al. 2009). In diseased explants, contributions from both myofibroblastic and osteogenic processes are present; dystrophic calcification and ossification has been observed in 83% and 13% of explanted diseased valves, respectively (Mohler et al. 2001). The details concerning how these stimuli work together to activate AVICs and produce the CAVD phenotype, however, remain largely unknown.

The mechanical cues that AVICs respond to are not limited to substrate composition and stiffness, and mechanical strain during the cardiac cycle may also contribute to CAVD. *In vivo*, compliance changes in the aortic wall alter the deformation profile of aortic valve leaflets. Under normal physiological conditions, the perimeter of the aortic valve annulus increases approximately 15% at the beginning of diastole, which allows for maximum radial deformation (Robicsek and Thubrikar 2002; Merryman 2009). However, with age the aorta stiffens (Haskett et al. 2010), causing the annulus to stiffen, minimizing the radial strain. This results in higher loads and deformations in the circumferential collagen fibers, the principle axis along which AVICs reside, and exposes them to greater mechanical strain. Studies exposing either AVICs or freshly excised, whole valve leaflets to varying levels or regimens of strain have shown responses such as structural changes to withstand this increased loading (Merryman et al. 2007b; Balachandran et al. 2006; Balachandran et al. 2009), but the effect of increased strain *in vivo* is unknown. Furthermore, few studies have used mechanical strain to investigate mineralization of AVICs to identify its role in CAVD (Balachandran et al. 2010; Merryman et al. 2007b; Simmons et al. 2004). Therefore, an investigation that applies strain in combination with other stimuli to impact AVIC calcification will provide new insights into the progression of CAVD.

To assess the extent strain mediates calcification of AVICs, we used an *in vitro* Flexcell system to apply varying levels of equibiaxial strain to AVICs in the presence or absence of TGF-β1. The incubation of TGF-β1 prior to the application of strain accelerated the nodule formation process by increasing monolayer tension that initiated aggregation and nodule maturation. Both TGF-β1 and mechanical strain revealed cell-cell adhesion forces that inhibited motility and promoted aggregates to calcify. Further, we identify a novel property of strain magnification using linear elasticity theory to better approximate the *in vitro* mechanical environment that supports calcific nodule growth. The results show that strain is an important contributor to nodule formation and regulates the mechanobiology of AVIC monolayers.

2. Methods and Materials

2.1. Cell Isolation and Culture

Porcine aortic valve leaflets were excised from sacrificed animals within 10 minutes of slaughter at a local abattoir. Leaflets were stored in phosphate buffered saline (PBS) at 4° C to ensure survival. Within 3 hours (h) of sacrifice, AVICs were isolated as previously described (Merryman et al. 2007a). Briefly, after the removal of the endothelium, the leaflet was diced and digested in a 1 mg/ml collagenase solution (Worthington Biochemical Corp., Lackwood, NJ) for 1 h at 37° C and 5% CO_2. The collagenase solution with the remaining tissue was passed through a cell strainer to collect a cell solution which was centrifuged at 1500 RPM for 5 min to obtain the cell pellet. The pellet was resuspended in Dulbecco's Modified Eagle Medium supplemented with 10% fetal bovine serum (Atlanta Biologicals; Lawrenceville, GA), 1% penicillin/streptomycin antibiotic (Cellgro; Manassas, VA), and 0.2% Amphotericin B (Sigma; St. Louis, MO). The cells were seeded into T-75 tissue culture flasks and incubated at 37° C and 5% CO_2 with media changes every three days. All cells were frozen for storage after the second passage.

2.2. Strain and TGF-β1 Treatments

AVICs were trypsinized at ~80% confluence, counted with a hemocytometer, and seeded onto Bioflex Pronectin culture plates (Flexcell International Corporation) at a density of 50,000 cells/cm^2 in 3 ml of media. No cellular aggregates preexisted during the cell counting or in culture. Cells were given 2 days to reach confluence in growth media and were then treated with 6 combinations of TGF-β1 and strain (Figure 1) over 48 h. Depending on the protocol, cultures were either treated with 1 ng/ml porcine TGF-β1 (R&D Systems; Minneapolis, MN) or kept in growth media. The media was changed daily during experimentation. For cultures undergoing strain, cells were subjected to cyclic equibiaxial strain via the Flexcell-4000 tension system (Flexcell International Corporation) at a frequency of 0.75 Hz, the maximum frequency for generating vacuums that ensure ≥15% strains each cycle. Various strain levels were applied using different diameter loading posts (Flexcell International Corporation). 5% (31 mm posts), 10% (28 mm), 15% (25 mm or 28 mm), and 20% (25 mm) strain were used in these experiments to represent a range that corresponds to both physiological and pathological strain levels. Control groups were incubated on Bioflex Pronectin culture plates in static conditions in the same tissue culture incubator housing the Flexcell system. All experiments were performed using AVICs spanning passages 4-7 with no apparent differences in results across these passages.

2.3. Calcific Nodule Quantification

After treatment, AVICs were rinsed twice with PBS and fixed in 3.7% neutral buffered formaldehyde for 15 min. AVICs were rinsed with PBS and, unless immediately stained, stored at 4°C for up to several days. Each 35 mm well was rinsed with deionized water (dH_2O) and stained with 1 ml of 14 mM Alizarin red S (Sigma) (in dH_2O, pH 4.1, where undissolved particulates were removed by brief centrifugation and then with a 0.45μm filter) for 30 min with agitation to determine calcium deposition. After staining, the cells were washed 4 times with dH_2O to remove excess dye. Positively stained nodules were manually counted under the microscope. Nodules were defined as round, having a minimum 100 μm diameter (twice that of the long axis of individual cells), sufficient staining intensity, containing elongated cells in a radial pattern around the periphery of the nodule, and adjacent to a region devoid of cells.

2.4. Enzyme-linked Immunosorbent Assay

After treatment, AVICs from all samples were incubated for 15 min at room temperature and then scraped in lysis buffer (Cell Lytic M (Sigma), 10% protease inhibitor cocktail (Sigma), 1% phosphatase inhibitor cocktail (Sigma)). Lysates were centrifuged at 16,000*g for 20 min and the top 80% volume of supernatant collected and stored at -80°C until use. Lysates from all samples were assayed for total protein content using a Bradford assay and diluted to a final protein concentration of 5 μg/ml in carbonate/bicarbonate buffer (pH 9.6) (Sigma). These antigen solutions were added to 96 well plates and incubated at RT overnight to allow the proteins to adsorb to the plate surface. αSMA was then quantified via ELISA (Merryman et al. 2006b). We confirmed antibody specificity using an αSMA peptide (Abnova; Walnut, CA) using standard Western blot, and our results are within the linear range of detection using this peptide in each ELISA assay performed (results not shown).

2.5. Wound Assay

AVICs were seeded onto standard 6 well tissue culture plastic plates or Flexcell Pronectin plates at a seeding density of 60,000 cells/cm^2 and allowed to reach confluence in normal growth media. The cells were treated with either 0, 1, or 5 ng/ml of TGF-β1 for 24 h. After treatment, the media was replaced with normal growth media. To apply the wound, a 200 μl pipette tip (diameter~820 μm) was used to create a cross-shaped incision through the monolayer. The wells were rinsed with fresh media to remove any floating, cellular debris. Images were acquired on a tissue culture microscope immediately after incision. Wound area was quantified in ImageJ. After selecting five approximately equal-spaced locations in the horizontal and vertical directions, separation distances were averaged to represent wound width and height and multiplied together to determine wound area.

2.6. Characterization of Apoptosis and Inhibition with ZVAD

AVICs were rinsed with PBS and stained with Annexin V conjugated with Alexa fluor 488 (5% solution in Annexin binding buffer; Invitrogen) for 15 minutes to detect apoptotic cells. Propidium Iodide (0.4% solution in Annexin binding buffer; Invitrogen) was used as a counter-stain for necrotic cells. Apoptosis and necrosis images were taken after 3, 12, and 24 h of equibiaxial strain using a fluorescence microscope (Nikon TE300 Inverted Tissue Culture Microscope).

Apoptosis inhibition studies were performed using ZVAD-FMK (R&D Systems), a general caspase inhibitor. After TGF-β1 supplemented media was removed from AVICs, media supplemented with ZVAD in concentrations of 20 or 50 μM was added to each well and incubated for 30 min prior to application of 15% strain.

2.7. Statistical Analysis

Results were analyzed as mean ± SE. ANOVA and Holm-Sidek tests were performed as needed. Statistical significance was defined as $p < 0.05$.

3. Results

3.1. Calcific Nodule Formation is Dependent on the Order of TGF-β1 and Mechanical Strain Treatment

We previously investigated the effects of TGF-β1 and mechanical strain on valve leaflets to test their role in the differentiation of AVICs into the myofibroblast phenotype (Merryman et al. 2007b; Balachandran et al. 2010). Also, there have been multiple other studies that have examined mechanical strain and TGF-β1 treatment on fibroblasts (Hinz et al. 2001;

Wipff et al. 2007; Tomasek et al. 2002; Goffin et al. 2006). The order of addition has been varied in multiple ways: simultaneous TGF-β1 incubation with strain (Merryman et al. 2007b; Balachandran et al. 2010), pretreatment with TGF-β1 for several days prior to application of strain (Goffin et al. 2006), and the application of mechanical tension prior to TGF-β1 incubation (Hinz et al. 2001; Wipff et al. 2007). Because it is speculated that myofibroblast differentiation precedes calcific nodule morphogenesis, we sought to test the order of addition of TGF-β1 and mechanical strain.

We exposed the AVICs to six combinations of TGF-β1 and strain over 48 hours and then stained the wells with alizarin red to detect the presence of calcific nodules. Static culture, TGF-β1, and strain alone did not generate calcific nodules after 48 h and only an unperturbed cell monolayer was observed (Fig. 1A-C). AVICs strained first for 24 h and then treated with TGF-β1 for 24 h generated no calcific nodules with only a monolayer observed (Fig. 1D); however, when AVICs were incubated first with TGF-β1 for 24 h and subsequently strained for the next 24 h, a large number of calcific nodules were generated, intensely stained with alizarin red (Fig. 1E). Simultaneous treatment of TGF-β1 and strain generated calcific nodules after 48 h; however, these nodules were smaller and faintly stained in comparison to the prior case (Fig. 1F). These results suggest that pretreating AVICs with TGF-β1 prior to strain produces the optimal nodule formation after 48 h. To our knowledge, static culture studies in the literature report aggregation and mature nodule formation occur between 3 days (Jian et al. 2003) and 3 weeks (Chen et al. 2009) after reaching confluence. Studies that utilize larger concentrations of TGF-β1 (≥ 5 ng/ml) observe nodule formation with shorter culture duration (Jian et al. 2003; Walker et al. 2004; Mohler et al. 1999) while others using lower concentrations of TGF-β1 or other media supplements require longer durations in culture (Benton et al. 2008; Chen et al. 2009; Rodriguez and Masters 2009) . Also, most studies are unclear about differentiating between initial aggregation events and the extent of calcification needed to define a nodule since this conversion can take over one week (Jian et al. 2003). Thus, a sequential treatment of TGF-β1 and strain appears to be most efficient for forming mature calcified nodules.

3.2. Variables Regulating Nodule Formation

To determine how TGF-β1 and mechanical strain influence nodule formation, we individually varied the concentration of TGF-β1 incubation and the extent of strain. First, we incubated AVICs with various TGF-β1 concentrations (0 – 5 ng/ml) and then applied 15% cyclic strain (Fig. 2A). We observed greater numbers of calcific nodules with increasing TGF-β1 concentrations, suggesting that the likelihood of nodule formation is actively regulated by changes to the cells induced by TGF-β1. To assess the role of mechanical strain, we pretreated AVICs with 1 ng/ml TGF-β1 for 24 h and then subjected them to different magnitudes of strain (0 – 20%). We observed increasing number of calcific nodules with increasing strain (Fig. 2B). We note that at lower levels of TGF-β1 and strain, amorphous cellular aggregates were observed that stained poorly with alizarin red and were not included in the nodule count. These results suggest that threshold levels of both TGF-β1 and strain are needed to produce mature nodules.

3.3. Mechanical Damage Reveals TGF-β1 Enhancement of AVIC Monolayer Tension

The response of statically cultured AVICs treated with TGF-β1 suggests that the aggregation process occurs via monolayer disruption due to αSMA mediated contractility (Benton et al. 2009). Because TGF-β1 incubation is well established at increasing αSMA expression in AVICs (Walker et al. 2004), we first wanted to assess how the 24 h TGF-β1 incubation affected the AVICs in our system. We used an ELISA assay to measure the expression of αSMA in these monolayers and observed a ~2.2 fold increase after 24 h that was dose-dependent (Fig. 3A). These results confirm that TGF-β1 induces the same

magnitude effect on the Bioflex Pronectin culture plates as tissue culture plastic (Walker et al. 2004).

After verifying the effect of TGF-β1 on αSMA expression, we tested how TGF-β1 alters the mechanics of the monolayer by subjecting AVIC cultures to a wound assay. Because greater αSMA expression increases contractility (Benton et al. 2009), we speculate that higher αSMA expression will translate to greater tension in the AVIC monolayer. AVICs treated with TGF-β1 opened larger wounds after the incision (Fig. 3B). This opening effect is not unique to monolayers cultured on the Flexcell membranes because a similar increase is observed for monolayers cultured on standard tissue culture plastic (Fig.3B). Interestingly, the wounds created in non-TGF-β1 treated wells were approximately the size of the pipette tip on both materials indicating that the tension in these monolayers is negligible and also that the cell-cell associations may be weak relative to cell-substrate interactions. Regardless of substrate, the increase in tension is due to TGF-β1, however, further increases in tension did not appear with larger doses of TGF-β1. This increase in tension could explain observations of monolayer disruption (Benton et al. 2009) and aggregation, particularly upon application of strain. Strain would then be insufficient to promote aggregates when the monolayer tension is small (Fig. 1B). The response of AVICs to TGF-β1 is likely not limited to an increase in monolayer tension in order to fully describe how it promotes nodule formation (Fig. 2A).

3.4. Time Course of Calcification: Nodule Maturation Spreads From Center Outward, From Early to Late Stage Apoptosis

To investigate how aggregates remodel into calcific nodules, we analyzed images at intermediate time points over the 24 h after initiating the application of strain. Because calcific nodules are associated with apoptotic processes (Yip et al. 2009; Jian et al. 2003; Mohler et al. 1999; Benton et al. 2008; Gu and Masters 2011), we speculated that apoptosis develops over time. Annexin V was used to stain the membranes of apoptotic cells, and propidum iodide (PI) was used to stain necrotic cells that have lost their cell membrane. Prior to application of strain, the monolayer treated with TGF-β1 sparsely binds either stain indicating cell viability (Fig. 4A). At 3 h, aggregates contain faint amounts of both stains, but at 12 h, necrotic cells were prominent towards the center of the aggregate, and many of the cells in the aggregate were apoptotic. After 24 h, the core of the nodule is mostly necrotic and the apoptotic AVICs only appear in an intense ring around the periphery of the nodule. Viable cells, which contain neither stain, appear to radiate out of the periphery of the nodule. This phenotype appears to dominate at the 24 hour time point and suggests that nodule maturity occurs from the inside and spreads to the edges with the transition from an apoptotic state to a necrotic state.

To determine if apoptosis is required for nodule maturation, we used the general caspase inhibitor ZVAD to inhibit apoptosis. ZVAD has previously been demonstrated to inhibit calcium deposition in nodules (Jian et al. 2003). AVICs were cultured in media supplemented with ZVAD for 30 min prior to application of 15% cyclic strain. After 24 h, ZVAD treated wells contain significantly fewer mature nodules (Fig. 4B). Larger concentrations of ZVAD did not statistically reduce nodules any further (data not shown). These wells also contain many amorphous regions of higher cell density, distinct from the monolayer, that resembled aggregates. These regions stained poorly with annexin and PI, suggesting they were mostly composed of living cells. These regions were adjacent to areas devoid of cells, flatter than mature nodules, and did not appear to have cells migrating out to reestablish the cell monolayer.

To verify that nodule maturation correlates with calcification, we stained samples with alizarin red at the same time points above (Fig. 5). We have previously observed that

fixation with formaldehyde results in non-specific or saturated alizarin red binding; therefore no fixation was used in order to distinguish variations in calcification with time. Alizarin red intensity increases with time in aggregates, which seems to parallel with the PI staining pattern. After 24 h, nodules contain an intense alizarin red staining indicating a high density of solid calcium deposition.

3.5. Nodule Maturation is Dependent on Mechanical Strain

Since the application of strain initiates aggregate formation, we wanted to determine if continuous exposure to strain promotes nodule maturation. After 24 h pretreatment with TGF-β1, AVIC monolayers were equibiaxially strained at 15% for 5 min to initiate aggregation. Strain was removed, and these samples were then left at static conditions for 24 h. At 3 h, aggregates were observed to still be present in the well (Fig. 6A). Around the aggregates, cells were migrating radially outward (Fig. 6A; arrows). Interestingly, samples under continuous cyclic strain for the same duration had far fewer migratory cells around the aggregates (Fig. 6B; arrow). This suggests that strain inhibits AVIC motility and tends to keep a large portion of the cells in the aggregate.

At 24 h, many AVICs continued to migrate out of the aggregates in the static condition to further distances relative to the center of the aggregate, and the aggregates also appear to have flattened out, blending in with the rest of the monolayer (Fig. 6C). In contrast, samples exposed to continuous strain had very limited cell migration from the aggregates resulting in a mature nodule phenotype (Fig. 6D). Staining of aggregates that appeared after 5 min of strain revealed a limited presence of necrosis and faint staining for apoptosis (Fig. 6E). As before, strain for 24 h led to a prominent apoptotic ring surrounding the necrotic core (Fig. 6F). TGF-β1 pretreated static samples not exposed to any strain over 24 h remained as a monolayer (Fig. 1C) and did not stain for apoptosis or necrosis (data not shown) having the same appearance as images taken at t=0. These results suggest that continuous cyclic strain regulates more than just causing mechanical damage to a monolayer, but also whether cells can emerge and migrate out of an aggregate. This also indicates that aggregation does not automatically proceed to nodule maturation because the cells do not undergo apoptosis. Furthermore, cyclic strain does seem to promote apoptosis and the likelihood of becoming the mature nodule phenotype indicative of mineralization.

4. Discussion

4.1. Strain Accelerates Calcific Nodule Formation and Mimics Dystrophic Calcification

While the dynamic mechanical environment of AVICs has been shown to influence both function and pathology, it was unclear, prior to the current study, whether mechanical strain contributes to calcification reminiscent of aortic valve disease. Most models of calcific nodule formation have not explored the role of mechanical strain in this process. By applying an equibiaxial strain field to confluent AVICs, we have identified that mechanical strain can both initiate and accelerate the aggregation of AVICs to form calcific nodules. We show that TGF-β1 and mechanical strain must be provided in a specific sequence in order to generate calcific nodules. Our results indicate a rapid onset of nodule formation, taking approximately 48 h from the beginning of treatment, for the formation of significant numbers of large, mature nodules (Fig. 1E, Fig. 4). These results suggest that AVIC differentiation and remodeling are active processes that occur with short exposure to TGF-β1 (24 h) and are revealed by the application of sufficient mechanical strain for an equivalent duration (24 h). This was confirmed using simultaneous exposure to TGF-β1 and strain, a closer mimic to the physiological environment (Fig. 1F). In this model, calcification results from cells in the aggregate undergoing apoptosis, consistent with a retrospective

study demonstrating that 83% of diseased heart valves in humans are indicative of dystrophic calcification (Mohler et al. 2001).

4.2. Strain Reveals TGF-β1 Mediated Remodeling of AVICs and Initiates Aggregation

Our results indicate that strain performs multiple roles in nodule formation. First, strain reveals TGF-β1 mediated remodeling of the cell monolayer. TGF-β1 increased αSMA expression in the monolayer (Fig. 3A). Higher αSMA expression in AVICs caused by TGF-β1 treatment has been shown to increase contractility on unconstrained collagen gels (Benton et al. 2009; Merryman et al. 2007a). On constrained substrates, we predicted higher contractility should functionally increase tension in the cell monolayer. These TGF-β1 effects were confirmed with a wound assay in which the wound area was larger with addition of TGF-β1, inferring enhanced contractility (Fig. 3B), and explaining how mechanical damage to the monolayer via strain initiates the formation of AVIC aggregates (Fig. 4A). Increasing contractility and monolayer tension must also be complemented with tight cell-cell associations. Once mechanical damage occurs, aggregates form because the energy from relieving the tension combined with adhesion strength between cells must be greater than adhesion of the cells with the underlying substrate. Evidence of TGF-β1 remodeling adherens junctions that both strengthens these associations and induces mechanical damage under stress (Follonier et al. 2008; Hinz et al. 2004; Pittet et al. 2008), may also be important for understanding how αSMA generated tension leads to the aggregation of a sheet of cells.

Common features that generate calcific nodules have been heavily dependent on the experimental context. To study calcific nodule formation via TGF-β1 pathway, most of the published studies were performed on tissue culture polystyrene or a minimum of 120 kPa stiffness. TGF-β1 stimulation of AVICs (Chen and Simmons 2011) is highly dependent on substrate stiffness, and the Flexcell silicone membranes (~930 kPa) in our study are a closer approximation to valve tissue stiffness (Merryman et al. 2006a). Further, when studies utilize a minimum of 5 ng/ml TGF-β1 treatment in static culture, nodules are observed within 2-5 days (Mohler et al. 1999; Walker et al. 2004). For lower or no TGF-β1 treatment in static culture, other studies observe fewer nodules within this time period and may require as long as 3 weeks (Rodriguez and Masters 2009; Chen et al. 2009) in culture to be characterized. Such aggregation events have been mostly explained in the context of contractility, and multiple studies that inhibit contractility have shown reduced nodule formation (Benton et al. 2009; Yip and Simmons 2011; Gu and Masters 2009; Kennedy et al. 2009). In combination with substrate stiffness and surface coatings that also play important roles, we speculate that the amount of TGF-β1 exposure and time in culture are separate variables that regulate AVICs responses. These variables may determine the generating of an imbalance of tension in the cell monolayer capable of the events needed for aggregation to occur and regulate the migratory capacity that determines whether aggregates dissipate. Our results demonstrate that when strain is applied, lower levels of TGF-β1 and shorter durations are just as sufficient to create the conditions that lead to nodule formation. These results support a paradigm that cell-generated forces and externally applied forces are both needed to reveal properties that better represent physiological conditions.

4.3. Strain Promotes Maturation of Calcific Nodule via Apoptosis

Another role of strain is its regulation of nodule maturation. By maintaining cyclical strain for 24 h, calcific nodules were more likely to form from initial aggregates (Fig. 4A and Fig. 6D and F). Aggregates under strain were more likely to undergo apoptosis and generate large necrotic cores that were consistent with staining for calcification (Fig. 5). These results suggest that aggregation does not automatically proceed to mineralization and additional

regulatory mechanisms govern this transition. Together, these data suggest that strain regulates AVIC behavior in multiple points of nodule development.

A common feature in nodule formation is the dependence on apoptosis. Studies that inhibit apoptosis reduced nodule formation, but the aggregation process still occurred (Jian et al. 2003). Interestingly, inhibition of contractility also reduced apoptosis and nodule formation (Gu and Masters 2010). The addition of strain in the present study shows that apoptosis occurs as early as 3 h after aggregation and becomes prominent after 12 h (Fig. 4A). In static cultures, similar apoptosis staining is observed after 5 – 7 days (Benton et al. 2008; Jian et al. 2003; Yip et al. 2009), while two studies showed that strain increases both apoptosis and calcification in valvular tissues (Balachandran et al. 2010) and vascular cells (Simmons et al. 2004). Our results show a dramatic and rapid conversion from apoptosis to necrosis in the central core of a mature nodule when strain is applied over the final 12 h. A very intense ring of apoptosis surrounds the periphery of the nodule, and, to our knowledge, has not been previously reported. We show that this conversion appears to be strain dependent and correlate with reduced cell migration from cells incorporated in the aggregate.

While our data and other current models can produce calcific nodules *in vitro*, it is not clear if these mechanisms can predict nodule formation that arises during CAVD *in vivo*. Tissue level studies of valve leaflets exposed to both TGF-β1 and pathological strain suggest that a homogeneous distribution of cells shift to a heterogeneous distribution of cell aggregates containing apoptotic cells (Balachandran et al. 2010), consistent with our model system. Many other groups have also found evidence correlating calcification and apoptosis in AVICs (Hutcheson et al. 2011; Rajamannan et al. 2011) that possibly explain the events occurring in 83% of diseased heart valves (Mohler et al. 2001). This compendium of evidence supports apoptosis as one mechanism that may contribute to this pathology. Many of the remaining challenges at the cellular level involve identification of the signaling pathways and enzymes that initiate calcification and its location, whether intracellular or extracellular in origin, and temporal changes occurring over decades (Piper et al. 2003; Weinberg et al. 2009) *in vivo*. Additional investigations are needed probing interactions between AVICs, endothelial cells (Weinberg et al. 2010), and other cell types that control these processes at the tissue level. To understand the impact of the mechanical environment on these mechanisms, we first need a better approximation how externally applied forces can change within an AVIC monolayer.

4.4. Calcific Nodule Maturation by Strain Magnification: Modified Lamé Solution

The line between physiological and pathological strain levels has been used as an explanation for the impact of high strain on nodule formation. At the tissue level, the line was drawn between 10% and 15% uniaxial strain as significant differences in calcification were observed (Balachandran et al. 2010), and we also observed a significant increase in nodule formation at 15% and 20% strain (Fig. 2B). Recognizing that nodule maturation occurs symmetrically from the center outward during exposure to strain (Fig. 4, Fig. 6) and that calcification must also change material properties, as predicted in multiscale models (Weinberg et al. 2009), it is unclear how small differences in strain magnitude generate such large effects. Using principles of linear elasticity, mechanical strain magnitudes can be calculated for the defined geometry of our experimental system to more closely approximate the mechanical environment. We use a modified Lamé solution of a thick-walled cylinder to calculate the strain field at the periphery of the nodule that becomes altered at the junction between two different materials. The model derivation, numerical predictions, and limitations are described in the Appendix. By assuming a circular disc that contains a small rigid core (Fig. 7A), the mechanical changes to the applied equibiaxial strain field provides a new hypothesis to examine the process of nodule formation. The strain fields shift from equibiaxial to uniaxial which necessitates that the strains increase in one orientation and

decrease or become compressive in the other orientation. For rigid cores, the radial strains can increase up to two-fold and eliminate circumferential strains whereas loss of contact and absence of cells increase circumferential strains at the expense of radial strains (Fig.7B, C, D).

With these numerical predictions, we can better account for the changes we observed in the monolayer when applying strain. Assuming a uniform monolayer has homogenous material properties, in contrast, a TGF-β1 treated monolayer should create an imbalance in tension due to local heterogeneity of contractility and remodeling of cell-cell contacts. Weak areas in the monolayer will more likely rip when challenged by externally applied forces, and regions with tighter cell-cell associations will be primed to become the foci where cell sheets would accumulate into aggregates and have sufficient rigidity to promote strain enhancement. As we have shown with TGF-β1 treatment and lower strains approximated to be physiological (Fig.2B), the monolayer seems to withstand these forces or aggregates dissipate resulting in fewer nodules formed (Fig. 6). However, we speculate that at pathological strains, the increased magnitude of strain due to the strain enhancement cannot be tolerated, increasing the propensity for creating greater numbers of nodules (Fig. 2). Furthermore, strain enhancement may also be responsible for triggering the biological changes necessary for apoptosis and perhaps the conversion to necrosis that can explain how the necrotic core spreads from the center outward. Fully mature nodules may also alter the strain field creating more aggregation events that feed this nodule and cause it to increase in diameter. These events could explain how strain would accelerate nodule maturation and form dense calcific nodules. More broadly, this concept of strain enhancement may also be applicable in other tissues that are exposed to cyclical strain such as myocardium and lung tissues. Scar tissue in these regions may have different material properties from the surrounding tissue, and this principle could explain pathological responses in terms of greater strains than would normally be expected. Identification of principles that can be tested at the 2D environment act as a first approximation that can be extrapolated to the 3D environment (Weinberg and Kaazempur Mofrad 2007).

4.5. Conclusion

Our results suggest multiple biological checkpoints that regulate nodule formation and can assist in explaining the causes of CAVD. The complex interplay of biological changes induced by TGF-β1 is revealed by mechanical strain (including cell tension, cell contacts, migration, apoptosis, necrosis, and calcification), arguing that multiple active processes must occur to create the final pathological phenotype. Future efforts that can better classify these phenotypes for human patients will provide more specific strategies for pharmacological treatment.

Acknowledgments

This work was supported by the AHA (09GRNT2010125) and NIH (HL094707), both to WDM. JC was supported by an AHA Pre-doctoral Fellowship (11PRE7990023).

8. Appendix

Because AVICs aggregate as sheets, the cell-cell adhesion strength is greater than the cell-surface adhesion strength, and we treat this problem as a planar representation. Therefore, the underlying assumptions are the same as plane stress problems in linear elasticity that have been foundational in determining strength of materials and predicting mechanical failure. We think this description is relevant for several stages of nodule development.

The classical Lamé solution to the thick-walled cylinder (1833) can be used to describe how a calcified nodule alters the equibiaxial strain field felt by surrounding cells in our assay. This solution is more commonly used to assess how internal and external pressures of a thin slice of a long cylinder translate into radial and circumferential stresses and strains. By reversing the signs of the pressure terms in the Lamé equations, we have a mathematical solution for an outer disc responding to internal and external stresses around a central circular core. We simplify the geometry of our system to two concentric discs: an inner disc containing the cellular aggregate/nodule and an outer ring of surrounding monolayer/tissue (Fig. 7A). Assuming the circular core is small, these equations can be simplified. Given a range of inner stress values at the periphery of this core, we can calculate both the magnitudes and the gradient of stress and strain with radial position.

This model makes three physically meaningful predictions (Fig. 7B). First, for a homogenous monolayer, when an external stress (σ_o) is balanced by an equal, in magnitude, and opposite, in direction, internal stress (σ_i) (Fig. 7B at $\sigma_i/\sigma_o=1$), there is an equibiaxial stress and strain field. Using the equation of equilibrium, both the radial and circumferential stresses would each be equal to this same magnitude. This requires both the radial and circumferential strains to be identical. The second prediction considers the presence of a nodule or any material which is rigid and non-deformable (Fig. 7B at $\sigma_i/\sigma_o=1.33$). The boundary condition of the AVICs in contact with the nodule must also be non-deforming. To balance the external stress while preventing deformation, the internal stress must increase to $4\sigma_o/3$, assuming an incompressible Poisson's ratio ($\nu=0.5$). Since the circumferential component of strain is a function of radial displacement, it is zero at the periphery of the nodule. However, the radial component of strain is the derivative of the displacement and becomes double the equibiaxial strain applied to the system. This magnification of strain decays to the equibiaxial strain within approximately seven nodule radii (Fig. 7C). The third prediction is when the AVICs are adjacent to but no longer in contact with the nodule (Fig. 7B at $\sigma_i/\sigma_o=0$). In this case, the internal stress is zero and can be likened to a ‘hole’, an absence of material, or a material that is infinitely compliant. The circumferential strain is quadrupled and the radial strain is compressive, at twice the magnitude of the equibiaxial strain (Fig. 7D). It is unlikely that such an extreme would be experienced in this model, but the presence of regions devoid of cells means that the forces cannot be distributed evenly through the monolayer and AVICs near this boundary would be mechanically challenged and perhaps initiate new foci for aggregation and nodule formation.

Besides greatly simplifying the complex three dimensional geometry of the heart valve, the key limitation of this model is the equations are for infinitesimal strains, meaning they are directly proportional to length ratio. Real descriptions of strain are nonlinear functions of length ratio. Interestingly, the trends predicted by the Lamé theory for length ratio are consistent with both more advanced strain representations and experimental measurements (Balestrini et al. ; David and Humphrey 2004; Mori et al. 2005) for the cases we have presented. While the magnitudes and decay lengths should be different in actual biological tissue due to both material properties and geometry, we expect these principles to hold true. For example, in the valve leaflet, pathological strain is mainly applied along the circumferential direction, but any rigid material (e.g. the nodule) should still enhance the strain profile while further emphasizing the critical role AVICs have in maintaining the integrity of the valve leaflet.

a = radius of aggregate

R = radius of the entire monolayer

r = radial distance, $a \leq r \leq R$

E_Y = Young's modulus of the monolayer

ν = Poisson's ratio of the monolayer

σ_0 = externally applied stress, due to pressure in the aorta during diastole

σ_i = internally applied stress, due to contractility of cells in the nodule or rigidity of the nodule

σ_r = radial stress

σ_θ = circumferential stress

ε_r = radial stress

ε_θ = circumferential stress

ε_Z = axial strain

u = displacement

The modified Lamé solution for external and internally applied tensile stresses:

$$\sigma_r(r) = \left[1/\left(R^2 - a^2\right)\right]\left[\left(R^2\sigma_o - a^2\sigma_i\right) - (\sigma_o - \sigma_i)(aR/r)^2\right] \quad (1)$$

$$\sigma_\theta(r) = \left[1/\left(R^2 - a^2\right)\right]\left[\left(R^2\sigma_o - a^2\sigma_i\right) + (\sigma_o - \sigma_i)(aR/r)^2\right] \quad (2)$$

$$\varepsilon_r(r) = (1/E_Y)\left[1/\left(R^2 - a^2\right)\right]\left[(1-\nu)\left(R^2\sigma_o - a^2\sigma_i\right) - (1+\nu)(\sigma_o - \sigma_i)(aR/r)^2\right] \quad (3)$$

$$\varepsilon_\theta(r) = (1/E_Y)\left[1/\left(R^2 - a^2\right)\right]\left[(1-\nu)\left(R^2\sigma_o - a^2\sigma_i\right) - (1+\nu)(\sigma_o - \sigma_i)(aR/r)^2\right] \quad (4)$$

$$\varepsilon_z = (-2\nu/E_Y)\left(R^2\sigma_o - a^2\sigma_i\right)/\left(R^2 - a^2\right) \quad (5)$$

$$u(r) = (1/E_Y)\left[r/\left(R^2 - a^2\right)\right]\left[(1-\nu)\left(R^2\sigma_o - a^2\sigma_i\right) + (1+\nu)(\sigma_o - \sigma_i)(aR/r)^2\right] \quad (6)$$

For($R >> a$):

$$\sigma_r(r) = \sigma_o - (\sigma_o - \sigma_i)(a/r)^2 \quad (7)$$

$$\sigma_\theta(r) = \sigma_o + (\sigma_o - \sigma_i)(a/r)^2 \quad (8)$$

$$\varepsilon_r(r) = (1/E_Y)\left[(1-\nu)\sigma_o - (1+\nu)(\sigma_o - \sigma_i)(a/r)^2\right] \quad (9)$$

$$\varepsilon_\theta(r) = (1/E_Y)\left[(1-v)\,\sigma_o + (1+v)\,(\sigma_o - \sigma_i)\,(a/r)^2\right] \quad (10)$$

$$\varepsilon_z = -2v\sigma_o/E_Y \quad (11)$$

$$u(r) = (r/E_Y)\left[(1-v)\,\sigma_o + (1+v)\,(\sigma_o - \sigma_i)\,(a/r)^2\right] \quad (12)$$

Equibiaxial case ($\sigma_i = \sigma_o$, $R >> a$):

$$\sigma_{eqb} = \sigma_o \quad (13)$$

$$\varepsilon_{eqb} = (1-v)\,\sigma_o/E_Y \quad (14)$$

Evaluating magnitudes normalized with the equibiaxial case at the periphery of the nodule for ($R >> a$):

$$\sigma_r(a)/\sigma_{eqb} = \sigma_i/\sigma_o \quad (15)$$

$$\sigma_\theta(a)/\sigma_{eqb} = 2 - (\sigma_i/\sigma_o) \quad (16)$$

$$\varepsilon_r(a)/\varepsilon_{eqb} = [(1+v)\,(\sigma_i/\sigma_o) - 2v]/(1-v) \quad (17)$$

$$\varepsilon_\theta(a)/\varepsilon_{eqb} = [2 - (1+v)\,(\sigma_i/\sigma_o)]/(1-v) \quad (18)$$

References

Balachandran K, Konduri S, Sucosky P, Jo H, Yoganathan AP. An ex vivo study of the biological properties of porcine aortic valves in response to circumferential cyclic stretch. Ann Biomed Eng. 2006; 34(11):1655–1665. doi:10.1007/s10439-006-9167-8. [PubMed: 17031600]

Balachandran K, Sucosky P, Jo H, Yoganathan AP. Elevated cyclic stretch alters matrix remodeling in aortic valve cusps: implications for degenerative aortic valve disease. Am J Physiol Heart Circ Physiol. 2009; 296(3):H756–764. doi:00900.2008 [pii] 10.1152/ajpheart.00900.2008. [PubMed: 19151254]

Balachandran K, Sucosky P, Jo H, Yoganathan AP. Elevated cyclic stretch induces aortic valve calcification in a bone morphogenic protein-dependent manner. Am J Pathol. 2010; 177(1):49–57. doi:ajpath.2010.090631 [pii] 10.2353/ajpath.2010.090631. [PubMed: 20489151]

Balestrini JL, Skorinko JK, Hera A, Gaudette GR, Billiar KL. Applying controlled non-uniform deformation for in vitro studies of cell mechanobiology. Biomech Model Mechanobiol. 2010; 9(3): 329–344. doi:10.1007/s10237-009-0179-9. [PubMed: 20169395]

Benton JA, Kern HB, Anseth KS. Substrate properties influence calcification in valvular interstitial cell culture. J Heart Valve Dis. 2008; 17(6):689–699. [PubMed: 19137803]

Benton JA, Kern HB, Leinwand LA, Mariner PD, Anseth KS. Statins block calcific nodule formation of valvular interstitial cells by inhibiting alpha-smooth muscle actin expression. Arterioscler Thromb Vasc Biol. 2009; 29(11):1950–1957. doi:ATVBAHA.109.195271 [pii] 10.1161/ATVBAHA.109.195271. [PubMed: 19679827]

Chen JH, Chen WL, Sider KL, Yip CY, Simmons CA. beta-catenin mediates mechanically regulated, transforming growth factor-beta1-induced myofibroblast differentiation of aortic valve interstitial cells. Arterioscler Thromb Vasc Biol. 31(3):590–597. doi:ATVBAHA.110.220061 [pii] 10.1161/ATVBAHA.110.220061. [PubMed: 21127288]

Chen JH, Simmons CA. Cell-matrix interactions in the pathobiology of calcific aortic valve disease: critical roles for matricellular, matricrine, and matrix mechanics cues. Circ Res. 2011; 108(12): 1510–1524. doi:108/12/1510 [pii] 10.1161/CIRCRESAHA.110.234237. [PubMed: 21659654]

Chen JH, Yip CY, Sone ED, Simmons CA. Identification and characterization of aortic valve mesenchymal progenitor cells with robust osteogenic calcification potential. Am J Pathol. 2009; 174(3):1109–1119. doi:S0002-9440(10)60968-6 [pii] 10.2353/ajpath.2009.080750. [PubMed: 19218344]

Cushing MC, Liao JT, Anseth KS. Activation of valvular interstitial cells is mediated by transforming growth factor-beta1 interactions with matrix molecules. Matrix Biol. 2005; 24(6):428–437. [PubMed: 16055320]

David G, Humphrey JD. Redistribution of stress due to a circular hole in a nonlinear anisotropic membrane. J Biomech. 2004; 37(8):1197–1203. doi:10.1016/j.jbiomech.2003.12.013 S0021929003004676 [pii]. [PubMed: 15212925]

Follonier L, Schaub S, Meister JJ, Hinz B. Myofibroblast communication is controlled by intercellular mechanical coupling. J Cell Sci. 2008; 121(Pt 20):3305–3316. doi:jcs.024521 [pii] 10.1242/jcs.024521. [PubMed: 18827018]

Goffin JM, Pittet P, Csucs G, Lussi JW, Meister JJ, Hinz B. Focal adhesion size controls tension-dependent recruitment of alpha-smooth muscle actin to stress fibers. J Cell Biol. 2006; 172(2): 259–268. doi:jcb.200506179 [pii] 10.1083/jcb.200506179. [PubMed: 16401722]

Goldbarg SH, Elmariah S, Miller MA, Fuster V. Insights into degenerative aortic valve disease. J Am Coll Cardiol. 2007; 50(13):1205–1213. doi:S0735-1097(07)02135-3 [pii] 10.1016/j.jacc.2007.06.024. [PubMed: 17888836]

Gu X, Masters KS. Role of the MAPK/ERK pathway in valvular interstitial cell calcification. Am J Physiol Heart Circ Physiol. 2009; 296(6):H1748–1757. doi:00099.2009 [pii] 10.1152/ajpheart.00099.2009. [PubMed: 19363136]

Gu X, Masters KS. Regulation of valvular interstitial cell calcification by adhesive peptide sequences. J Biomed Mater Res A. 2010; 93(4):1620–1630. doi:10.1002/jbm.a.32660. [PubMed: 20073077]

Gu X, Masters KS. Role of the Rho pathway in regulating valvular interstitial cell phenotype and nodule formation. Am J Physiol Heart Circ Physiol. 2011; 300(2):H448–458. doi:ajpheart.01178.2009 [pii] 10.1152/ajpheart.01178.2009. [PubMed: 21131478]

Haskett D, Johnson G, Zhou A, Utzinger U, Vande Geest J. Microstructural and biomechanical alterations of the human aorta as a function of age and location. Biomech Model Mechanobiol. 2010; 9(6):725–736. doi:10.1007/s10237-010-0209-7. [PubMed: 20354753]

Helske S, Kupari M, Lindstedt KA, Kovanen PT. Aortic valve stenosis: an active atheroinflammatory process. Curr Opin Lipidol. 2007; 18(5):483–491. doi:10.1097/MOL.0b013e3282a66099 00041433-200710000-00002 [pii]. [PubMed: 17885417]

Hinz B, Mastrangelo D, Iselin CE, Chaponnier C, Gabbiani G. Mechanical tension controls granulation tissue contractile activity and myofibroblast differentiation. Am J Pathol. 2001; 159(3):1009–1020. doi:S0002-9440(10)61776-2 [pii] 10.1016/S0002-9440(10)61776-2. [PubMed: 11549593]

Hinz B, Pittet P, Smith-Clerc J, Chaponnier C, Meister JJ. Myofibroblast development is characterized by specific cell-cell adherens junctions. Mol Biol Cell. 2004; 15(9):4310–4320. doi:10.1091/mbc.E04-05-0386 E04-05-0386 [pii]. [PubMed: 15240821]

Hutcheson JD, Venkataraman R, Baudenbacher FJ, Merryman WD. Intracellular Ca(2+) accumulation is strain-dependent and correlates with apoptosis in aortic valve fibroblasts. J Biomech. 2011 doi:S0021-9290(11)00713-5 [pii] 10.1016/j.jbiomech.2011.11.031.

Jian B, Narula N, Li QY, Mohler ER 3rd, Levy RJ. Progression of aortic valve stenosis: TGF-beta1 is present in calcified aortic valve cusps and promotes aortic valve interstitial cell calcification via apoptosis. Ann Thorac Surg. 2003; 75(2):457–465. discussion 465-456. [PubMed: 12607654]

Kennedy JA, Hua X, Mishra K, Murphy GA, Rosenkranz AC, Horowitz JD. Inhibition of calcifying nodule formation in cultured porcine aortic valve cells by nitric oxide donors. Eur J Pharmacol. 2009; 602(1):28–35. doi:S0014-2999(08)01177-1 [pii] 10.1016/j.ejphar.2008.11.029. [PubMed: 19056377]

Merryman WD. What modulates the aortic valve interstitial cell phenotype? Future Cardiol. 2008; 4(3):247–252. doi:10.2217/14796678.4.3.247. [PubMed: 19804329]

Merryman WD. Mechano-potential etiologies of aortic valve disease. J Biomech. 2009; 43(1):87–92. doi:S0021-9290(09)00504-1 [pii] 10.1016/j.jbiomech.2009.09.013. [PubMed: 19811785]

Merryman WD, Huang HY, Schoen FJ, Sacks MS. The effects of cellular contraction on aortic valve leaflet flexural stiffness. J Biomech. 2006a; 39(1):88–96. doi:S0021-9290(04)00540-8 [pii] 10.1016/j.jbiomech.2004.11.008. [PubMed: 16271591]

Merryman WD, Liao J, Parekh A, Candiello JE, Lin H, Sacks MS. Differences in tissue-remodeling potential of aortic and pulmonary heart valve interstitial cells. Tissue Eng. 2007a; 13(9):2281–2289. doi:10.1089/ten.2006.0324. [PubMed: 17596117]

Merryman WD, Lukoff HD, Long RA, Engelmayr GC Jr. Hopkins RA, Sacks MS. Synergistic effects of cyclic tension and transforming growth factor-beta1 on the aortic valve myofibroblast. Cardiovasc Pathol. 2007b; 16(5):268–276. doi:S1054-8807(07)00053-1 [pii] 10.1016/j.carpath.2007.03.006. [PubMed: 17868877]

Merryman WD, Youn I, Lukoff HD, Krueger PM, Guilak F, Hopkins RA, Sacks MS. Correlation between heart valve interstitial cell stiffness and transvalvular pressure: implications for collagen biosynthesis. Am J Physiol Heart Circ Physiol. 2006b; 290(1):H224–231. [PubMed: 16126816]

Mohler ER 3rd, Chawla MK, Chang AW, Vyavahare N, Levy RJ, Graham L, Gannon FH. Identification and characterization of calcifying valve cells from human and canine aortic valves. J Heart Valve Dis. 1999; 8(3):254–260. [PubMed: 10399657]

Mohler ER 3rd, Gannon F, Reynolds C, Zimmerman R, Keane MG, Kaplan FS. Bone formation and inflammation in cardiac valves. Circulation. 2001; 103(11):1522–1528. [PubMed: 11257079]

Mori D, David G, Humphrey JD, Moore JE Jr. Stress distribution in a circular membrane with a central fixation. J Biomech Eng. 2005; 127(3):549–553. [PubMed: 16060363]

Piper C, Bergemann R, Schulte HD, Koerfer R, Horstkotte D. Can progression of valvar aortic stenosis be predicted accurately? Ann Thorac Surg. 2003; 76(3):676–680. discussion 680. doi:S0003497503005666 [pii]. [PubMed: 12963175]

Pittet P, Lee K, Kulik AJ, Meister JJ, Hinz B. Fibrogenic fibroblasts increase intercellular adhesion strength by reinforcing individual OB-cadherin bonds. J Cell Sci. 2008; 121(Pt 6):877–886. doi:jcs.024877 [pii] 10.1242/jcs.024877. [PubMed: 18303045]

Rajamannan NM. Mechanisms of aortic valve calcification: the LDL-density-radius theory: a translation from cell signaling to physiology. Am J Physiol Heart Circ Physiol. 2010; 298(1):H5–15. doi:00824.2009 [pii] 10.1152/ajpheart.00824.2009. [PubMed: 19855055]

Rajamannan NM, Evans FJ, Aikawa E, Grande-Allen KJ, Demer LL, Heistad DD, Simmons CA, Masters KS, Mathieu P, O'Brien KD, Schoen FJ, Towler DA, Yoganathan AP, Otto CM. Calcific aortic valve disease: not simply a degenerative process: A review and agenda for research from the National Heart and Lung and Blood Institute Aortic Stenosis Working Group. Executive summary: Calcific aortic valve disease-2011 update. Circulation. 2011; 124(16):1783–1791. doi:124/16/1783 [pii] 10.1161/CIRCULATIONAHA.110.006767. [PubMed: 22007101]

Robicsek F, Thubrikar MJ. Mechanical stress as cause of aortic valve disease. Presentation of a new aortic root prosthesis. Acta Chir Belg. 2002; 102(1):1–6. [PubMed: 11925731]

Rodriguez KJ, Masters KS. Regulation of valvular interstitial cell calcification by components of the extracellular matrix. J Biomed Mater Res A. 2009; 90(4):1043–1053. doi:10.1002/jbm.a.32187. [PubMed: 18671262]

Roger VL, Go AS, Lloyd-Jones DM, Adams RJ, Berry JD, Brown TM, Carnethon MR, Dai S, de Simone G, Ford ES, Fox CS, Fullerton HJ, Gillespie C, Greenlund KJ, Hailpern SM, Heit JA, Ho PM, Howard VJ, Kissela BM, Kittner SJ, Lackland DT, Lichtman JH, Lisabeth LD, Makuc DM, Marcus GM, Marelli A, Matchar DB, McDermott MM, Meigs JB, Moy CS, Mozaffarian D, Mussolino ME, Nichol G, Paynter NP, Rosamond WD, Sorlie PD, Stafford RS, Turan TN, Turner MB, Wong ND, Wylie-Rosett J. Heart disease and stroke statistics--2011 update: a report from the

American Heart Association. Circulation. 2011; 123(4):e18–e209. doi:CIR.0b013e3182009701 [pii] 10.1161/CIR.0b013e3182009701. [PubMed: 21160056]

Simmons CA, Nikolovski J, Thornton AJ, Matlis S, Mooney DJ. Mechanical stimulation and mitogen-activated protein kinase signaling independently regulate osteogenic differentiation and mineralization by calcifying vascular cells. J Biomech. 2004; 37(10):1531–1541. doi:10.1016/j.jbiomech.2004.01.006 S0021929004000351 [pii]. [PubMed: 15336928]

Tomasek JJ, Gabbiani G, Hinz B, Chaponnier C, Brown RA. Myofibroblasts and mechano-regulation of connective tissue remodelling. Nat Rev Mol Cell Biol. 2002; 3(5):349–363. doi:10.1038/nrm809 nrm809 [pii]. [PubMed: 11988769]

Walker GA, Masters KS, Shah DN, Anseth KS, Leinwand LA. Valvular myofibroblast activation by transforming growth factor-beta: implications for pathological extracellular matrix remodeling in heart valve disease. Circ Res. 2004; 95(3):253–260. doi:10.1161/01.RES.0000136520.07995.aa 01.RES.0000136520.07995.aa [pii]. [PubMed: 15217906]

Weinberg EJ, Kaazempur Mofrad MR. Transient, three-dimensional, multiscale simulations of the human aortic valve. Cardiovasc Eng. 2007; 7(4):140–155. doi:10.1007/s10558-007-9038-4. [PubMed: 18026835]

Weinberg EJ, Mack PJ, Schoen FJ, Garcia-Cardena G, Kaazempur Mofrad MR. Hemodynamic environments from opposing sides of human aortic valve leaflets evoke distinct endothelial phenotypes in vitro. Cardiovasc Eng. 2010; 10(1):5–11. doi:10.1007/s10558-009-9089-9. [PubMed: 20107896]

Weinberg EJ, Schoen FJ, Mofrad MR. A computational model of aging and calcification in the aortic heart valve. PLoS One. 2009; 4(6):e5960. doi:10.1371/journal.pone.0005960. [PubMed: 19536285]

Wipff PJ, Rifkin DB, Meister JJ, Hinz B. Myofibroblast contraction activates latent TGF-β1 from the extracellular matrix. J Cell Biol. 2007; 179(6):1311–1323. doi:jcb.200704042 [pii] 10.1083/jcb.200704042. [PubMed: 18086923]

Yip CY, Chen JH, Zhao R, Simmons CA. Calcification by valve interstitial cells is regulated by the stiffness of the extracellular matrix. Arterioscler Thromb Vasc Biol. 2009; 29(6):936–942. doi:ATVBAHA.108.182394 [pii] 10.1161/ATVBAHA.108.182394. [PubMed: 19304575]

Yip CY, Simmons CA. The aortic valve microenvironment and its role in calcific aortic valve disease. Cardiovasc Pathol. 2011; 20(3):177–182. doi:S1054-8807(10)00194-8 [pii] 10.1016/j.carpath.2010.12.001. [PubMed: 21256052]

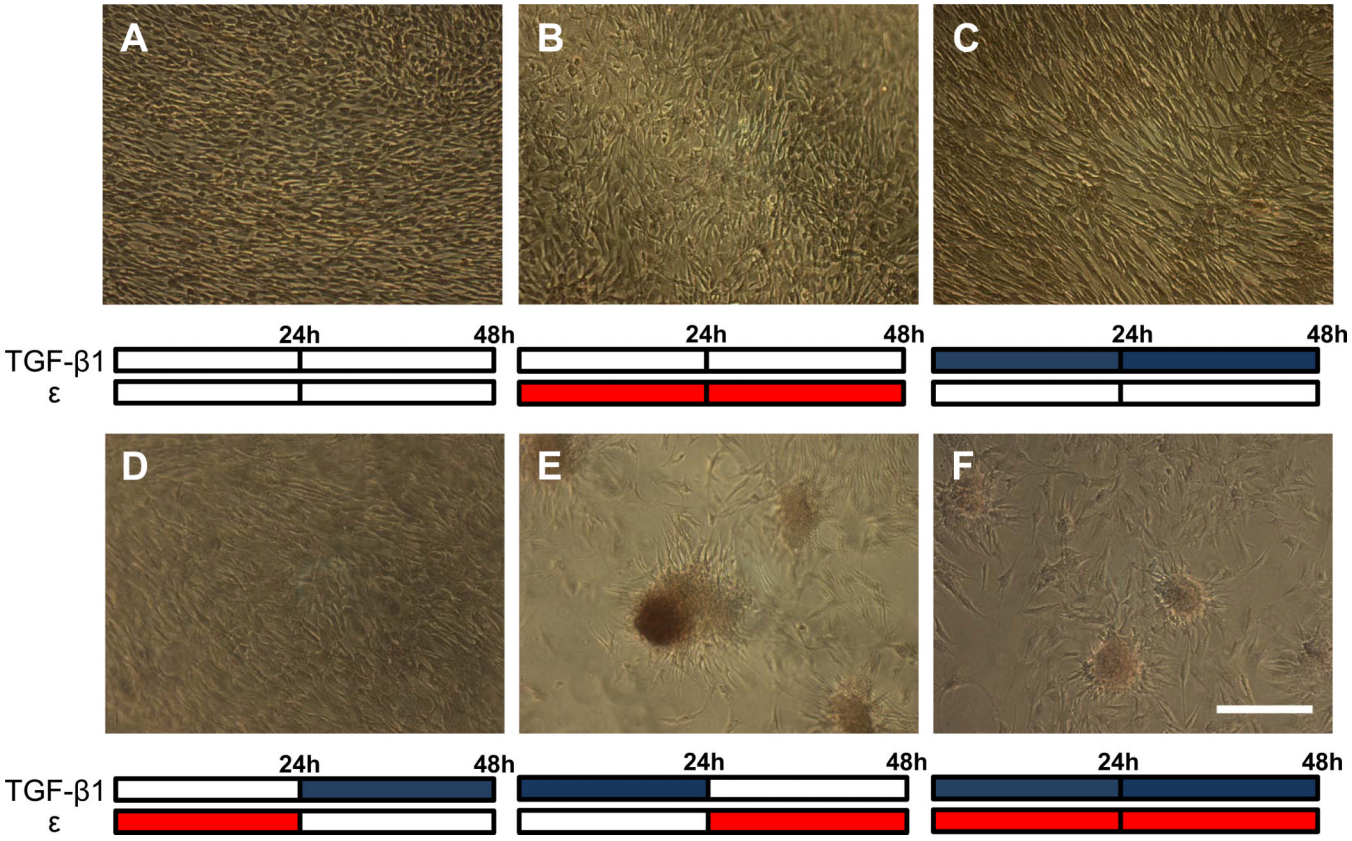

Fig. 1.

Calcific nodule formation following combination treatments of 15% equibiaxial strain (red bars) and 1 ng/ml of TGF-β1 (blue bars) over 48 hrs. Control (A), strain only (B), and TGF-β1 only (C) all show unperturbed monolayers, as does strain followed by TGF-β1 (D). TGF-β1 followed by strain reveals large, mature calcific nodules (E), while simultaneous TGF-β1 and strain cause small, less mature nodules (F). All treatments stained with Alizarin red to identify calcification. This experiment was independently replicated three times with identical results. Scale bar = 250 μm.

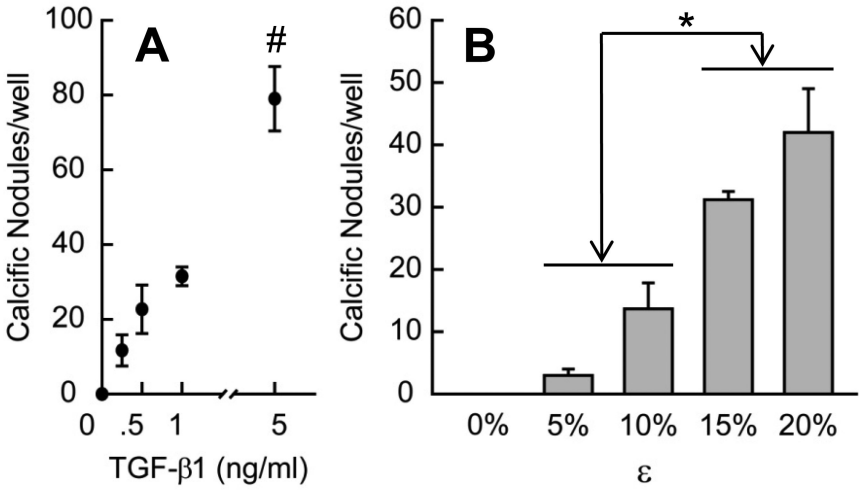

Fig. 2.

Nodule formation as a function of TGF-β1 concentration (A) and strain magnitude (B). For A, 24 h of 15% equibiaxial strain was applied after 24 h of each TGF-β1 concentration. For B, all groups were treated with 1 ng/ml TGF-β1 for 24 h prior to each strain being applied for 24 h. All bar graphs and points represent mean ± SE ($n \geq 3$), * = $p<0.05$, # = $p<0.01$.

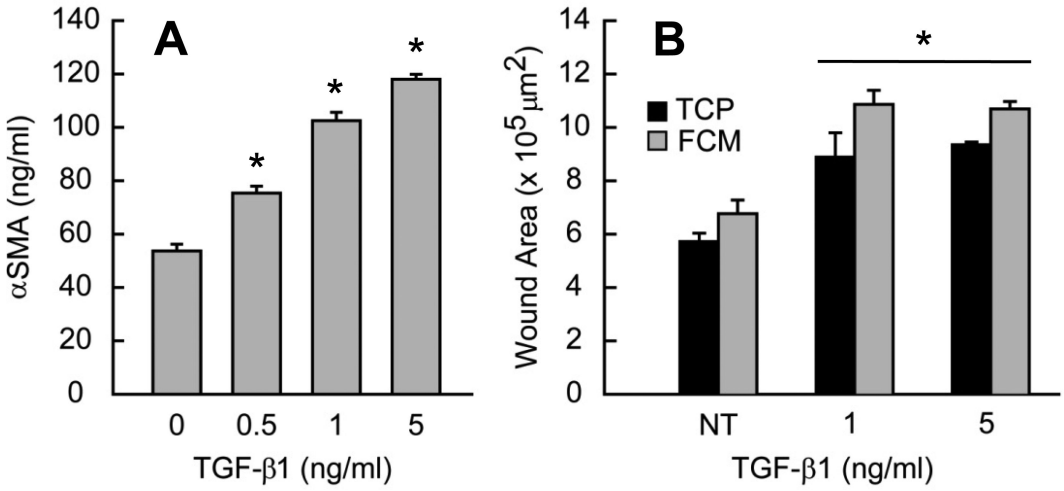

Fig. 3.

(A) aSMA expression increases with increasing dose of TGF-β1. (B) Mechanical damage reveals TGF-β1 effects on monolayer integrity. Monolayers were scraped with a 200 μl pipette tip in a cross pattern. Initial wound area increases with TGF-β1 pretreatment on tissue culture plastic (TCP) and Flexcell membrane (FCM). All bar graphs and points represent mean ± SE (n≥2), * = $p<0.05$.

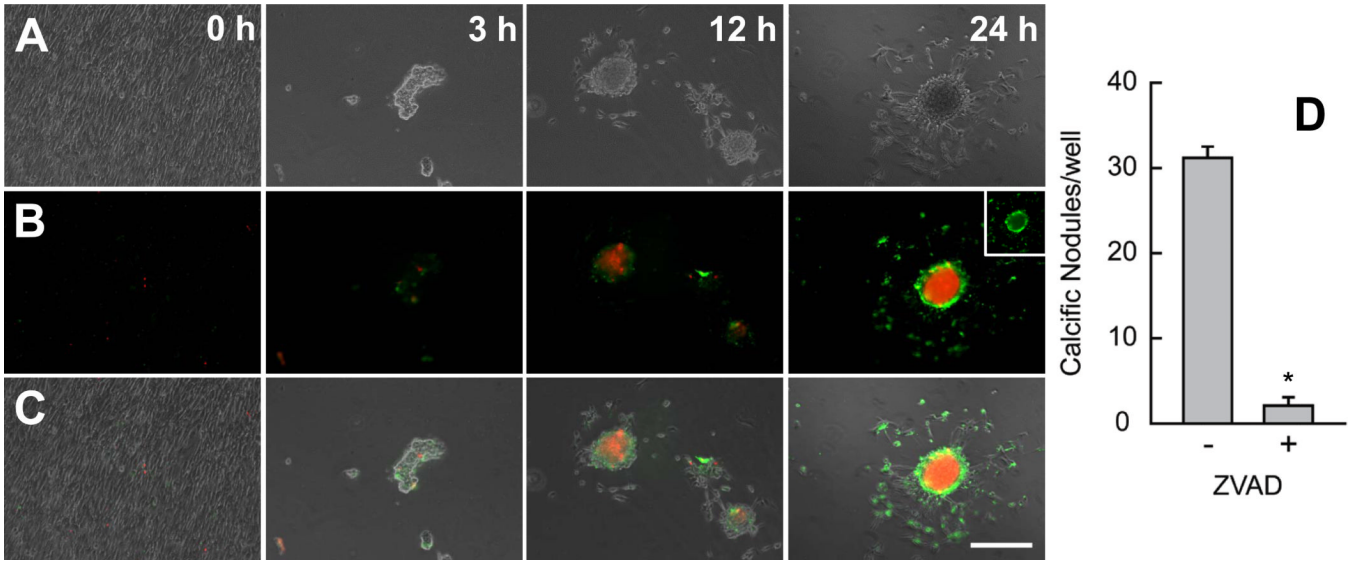

Fig. 4.

Nodule maturation spreads from the inside out and is dependent on apoptosis. Cultures were removed from strain at 3, 12, and 24 h and stained with Annexin V and propidium iodide (red) to identify apoptosis and necrosis respectively. Phase only (A), fluorescence only (B), phase and fluorescence overlay (C). Lack of stain at 0 h indicates cell viability and monolayer integrity. Stain intensity increases with time as apoptosis is replaced by an intense necrotic core. Inset represents green channel only showing apoptotic ring at the nodule periphery. Inhibition of apoptosis with ZVAD reduces the number of mature nodules per well (D). This experiment was independently replicated three times with identical results. * = $p<0.05$. Scale bar = 250 μm.

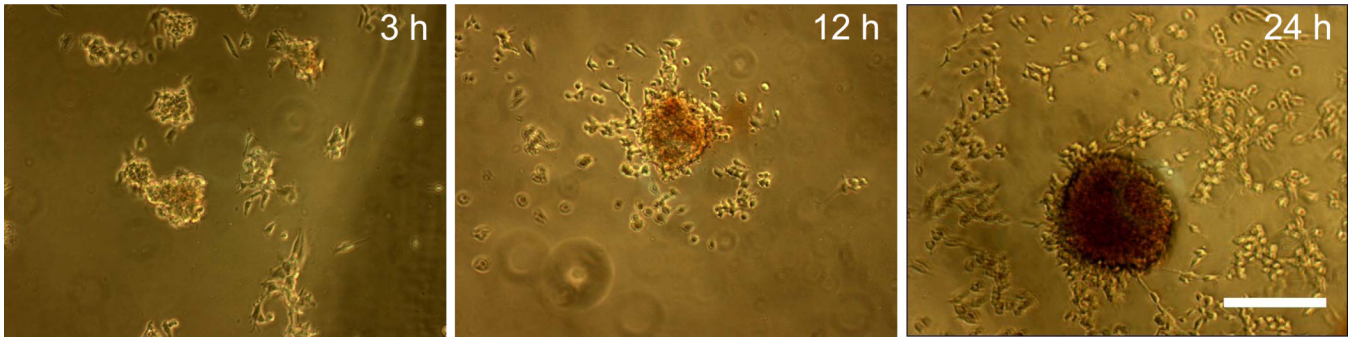

Fig. 5.

Nodules calcification occurs concomitantly with maturation. Cultures were removed from strain at 3, 12, and 24 h and stained with alizarin red. Stain increases intensity with time. No fixation was used prior to staining causing cells to round up. A minimum of 3 wells were observed for each case. Scale bar = 250 μm.

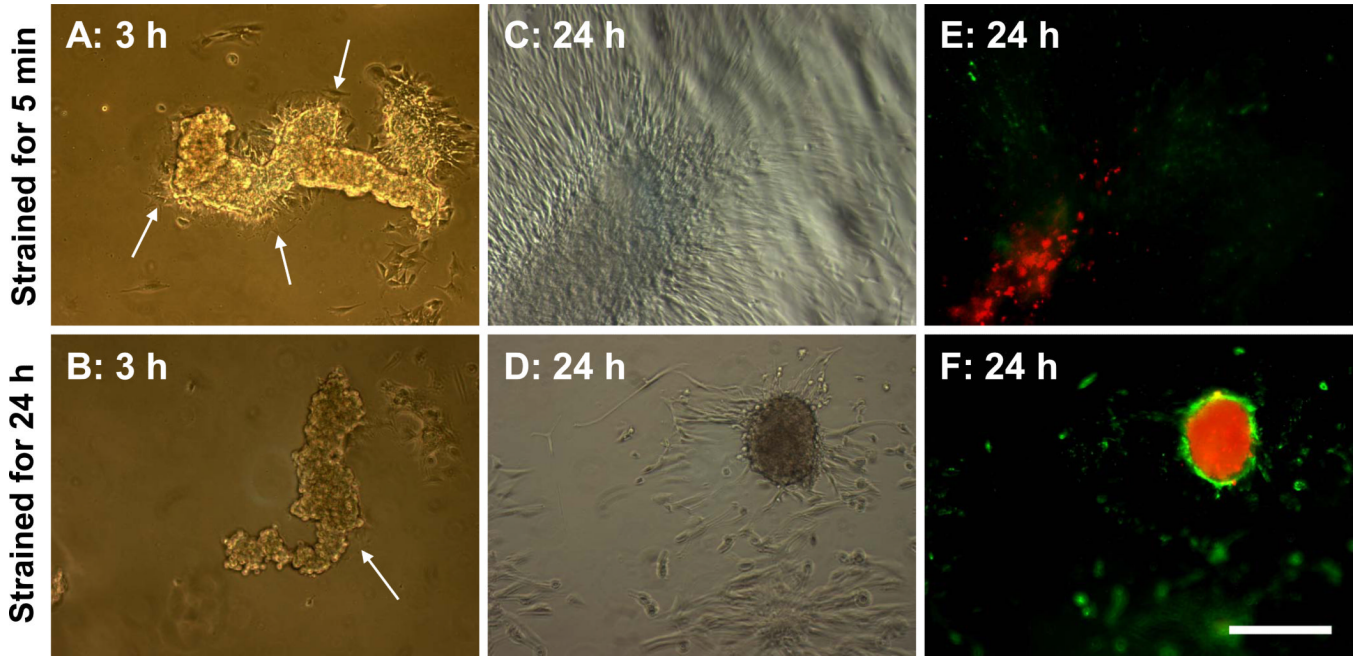

Fig. 6.

Nodule maturation is strain dependent. Aggregation was induced with exposure to 5 min of strain. Cultures were either removed from strain (A, C, E) or continued to receive cyclic strain for 24 h (B, D, F). Images were collected at 3 and 24 h and stained with Annexin V and propidium iodide (red) to identify apoptosis and necrosis respectively. Arrows point to AVIC migration emerging from the aggregate but seem to be inhibited with strain. Flattened aggregates with minimal apoptotic staining (E) were not observed in cultures under 24 h strain. This experiment was independently replicated three times with identical results. Scale bar = 250 μm.

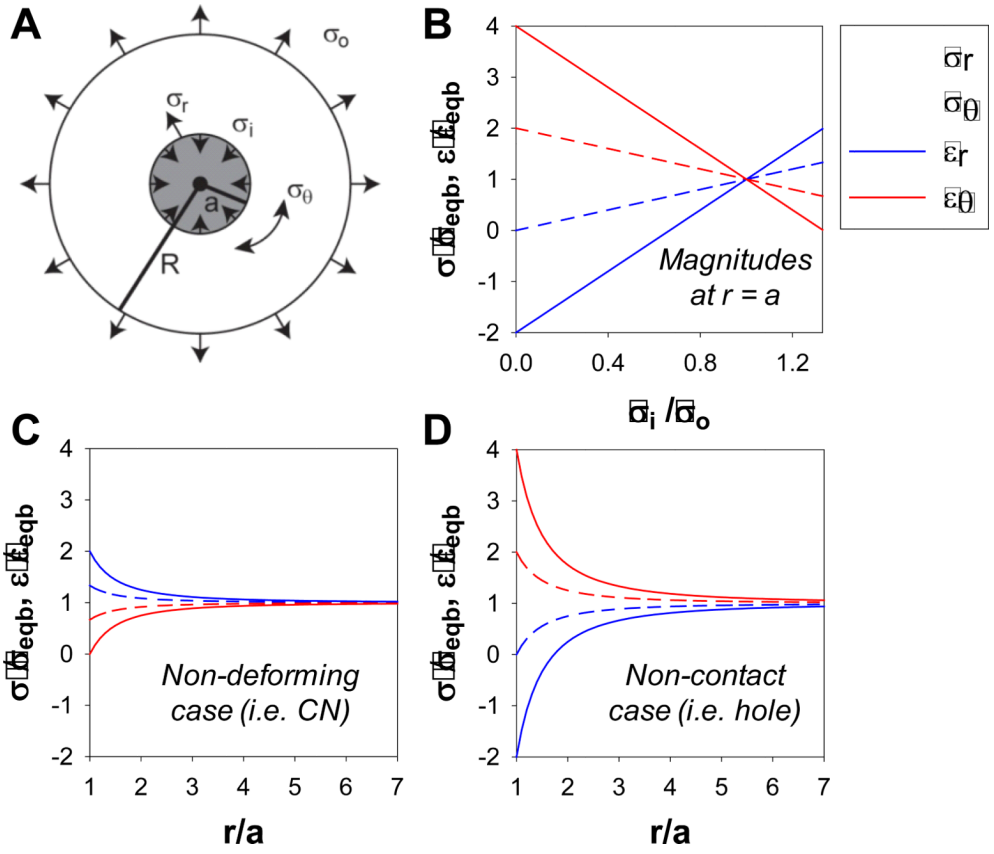

Fig. 7.

Strain enhancement model: Modified Lamé solution. External (σ_o) and internal (σ_i) stresses applied to a ring (radius = R) surrounding a circular core (radius = a) (A) used to calculate radial and circumferential stresses and strains at the core periphery (r = a) normalized to the equibiaxial case (B). Normalized gradient of stresses and strains as a function of the core radius were calculated for the non-deforming case ($\sigma_i = 4\sigma_o/3$) (C) and the non-contact case ($\sigma_i = 0$) (D). For all cases, R >> a. Normalized magnitudes indicate the extent of magnification of applied stresses and strains at the periphery of the circular core suggesting how small increases in strain can have significant impact on cells.